NASA Contractor Report 191170

Inelastic Deformation Mechanisms in SCS-6/Ti 15–3 MMC Lamina Under Compression

Golam M. Newaz and Bhaskar S. Majumdar
Battelle Memorial Institute
Columbus, Ohio

September 1993

Prepared for
Lewis Research Center
Under Contract NAS3–26494

National Aeronautics and Space Administration

INELASTIC DEFORMATION MECHANISMS IN SCS-6/Ti 15-3 MMC LAMINA UNDER COMPRESSION

Golam M. Newaz and Bhaskar S. Majumdar**
Battelle Memorial Institute
Columbus, Ohio 43201

ABSTRACT

An investigation was undertaken to study the inelastic deformation mechanisms in $[0]_8$ and $[90]_8$ Ti 15-3/SCS-6 lamina subjected to pure compression. Monotonic tests were conducted at room temperature (RT), 538°C and 650°C. Results indicate that mechanical response and deformation characteristics were different in monotonic tension and compression loading whereas some of those differences could be attributed to residual stress effects. There were other differences because of changes in damage and failure modes. The inelastic deformation in the $[0]_8$ lamina under compression was controlled primarily by matrix plasticity, although some evidence of fiber-matrix debonding was observed. Failure of the specimen in compression was due to fiber buckling in a macroscopic shear zone (the failure plane). The inelastic deformation mechanisms under compression in $[90]_8$ lamina were controlled by radial fiber fracture, matrix plasticity and fiber-matrix debonding. The radial fiber fracture was a new damage mode observed for MMCs. Constitutive response was predicted for both the $[0]_8$ and $[90]_8$ laminae, using AGLPLY, METCAN and Battelle's Unit Cell FEA model. Results from the analyses were encouraging.

INTRODUCTION

Titanium based metal matrix composites (MMCs) offer excellent potential for high temperature applications which require a combination of high temperature strength, stiffness and toughness. Current advances in processing of this class of materials have made them

** Currently with Universal Energy Systems, Inc., Dayton, Ohio

technologically viable for their use in various engine and aerothermal applications. Considerable research to date has been conducted in characterizing SiC fiber-reinforced titanium composites [1-9]. The references reflect only a small number of representative publications from a much larger pool.

An important feature of MMCs is that there is significant difference in the coefficient of thermal expansion between the fiber and matrix; the matrix has a larger coefficient of thermal expansion. Consequently, large compressive radial stresses build up at the interface between the matrix and the fiber as the composite is cooled from the processing temperature. Of course, fiber volume fraction affects the magnitude of the residual stresses. On the other hand, the axial and circumferential stresses in the matrix are both tensile in nature. This combination of stresses sets up yielding or near yielding conditions in the matrix immediately adjacent to the fiber. A consequence of such high stresses is that micro-yielding may occur well before macroscopic yield is observed when the MMC is loaded mechanically. In addition, the strength of the bond between the fiber and the matrix has been shown by many researchers [5,7,9] to be weak in the composite. Also, the presence of the reaction zone adds another dimension to the complex deformation characteristics in these composites under applied loading.

The loading mode which has received most attention by researchers in the field is tensile loading. Although, this is certainly the dominant loading mode for the application of the fiber reinforced MMCs, compressive loading in the application of these structural materials is a definite possibility for various components. Compression on one surface is a reality in bending. Furthermore, in the case of reversed fatigue loading, the composite will experience compressive loading in part of the cycle.

It is also anticipated that structural design engineers will require design allowables for tensile, compressive and shear properties. Compressive loading has not received much attention to date for high temperature composites. Past studies on Boron/Aluminum composites concentrated on their longitudinal compression behavior [10]; however, their transverse compression behavior was not studied. Understanding of the evolution of damage and failure modes under compressive loading of the MMC at high temperature is seriously lacking. Considerable research is needed to clarify and resolve the micromechanics issues

for compressive response. It is also necessary to complement experimental efforts with analytical ones to predict the constitutive response of the MMC under compressive loading since such efforts are not under consideration in any of the major high temperature programs.

Often damage accumulates in local regions in a structure due to high stresses and strains. If the damage reaches a critical level, it can lead to failure of the structure. Constitutive models are essential to evaluate local stress and strain fields developed due to global structural loading. However, rational constitutive models can be only developed if the mechanisms for material deformation and damage development can be clarified and used to develop the models. Analytical constitutive models often require an assumption of ideal microstructures and may simplify the problem to a level where realism is compromised, particularly for heterogeneous materials like composites. A computational framework on the other hand provides much versatility and can be effectively utilized provided deformation mechanisms are properly accounted for. For MMC structures subjected to compressive loading (a situation which exists even in the case of simple bending), constitutive modeling under compressive loading is a clearly defined need. Clarification of damage modes and deformation mechanisms are equally important compared with constitutive modeling and are integrally related. The material deformation characteristics and modeling for monotonic loading constitutes the basic requirements for structural analysis.

Inelastic deformation is critical in that its initiation and evolution contributes to the failure of a structural part. Proper constitutive models can only be developed when actual inelastic deformation mechanisms can be ascertained and incorporated into modeling.

In recognition of the need to clarify the inelastic deformation mechanisms under compressive loading, a brief investigation was undertaken to monitor the initiation and progression of damage in the SCS-6/Ti 15-3 MMC for both $[0]_8$ and $[90]_8$ laminae subjected to monotonic compressive loads, particularly at elevated temperature. This small effort was only part of a much larger effort for damage evaluation under cyclic loading in titanium-based MMCs which is covered in a separate report. This information will be extremely valuable for constitutive and damage modeling for this class of materials. Results were also compared with tension response and corresponding deformation mechanisms.

EXPERIMENTAL ASPECTS

The material tested was an 8-ply unidirectional SCS-6/Ti 15-3 composite, approximately 1.99-mm thick, with a fiber volume fraction of approximately 0.35. The SCS-6 (SiC) fiber diameter is approximately 140 μm, and it contains alternating outer layers of C and Si, which protect the fiber from damage during handling. The Ti 15-3 alloy is a metastable body centered cubic (bcc) beta Ti-alloy, the bcc phase being stabilized by V. The material is metastable because hexagonal close packed (hcp) alpha phase, which is the stable room temperature phase of pure Ti, precipitates when the material is held at temperatures as low as 400°C for long periods of time.

$[0]_8$ and $[90]_8$ rectangular test specimens were machined from the unidirectional panel using an electric-discharge machining (EDM) technique, with specimen dimensions of 2.0 mm x 10.2 mm x 104.1 mm. The gage length was 25.4 mm. The specimens were mechanically polished after EDM machining to minimize any damage associated with the machining. All specimens were tested in the as-fabricated condition, i.e., no heat-treatment was performed prior to the testing. Tests were conducted at room temperature, 538°C (1000°F) and 650°C (1200°F).

Specimens were gripped using friction grips, and loaded on a servohydraulic testing machine at a strain rate of approximately 0.004/sec. Compression testing was done using a Battelle developed compression fixture as shown in Figure 1 which uses buckling guides. The longitudinal strains were measured using extensometer.

A few tests were conducted without buckling guides, particularly for $[0]_8$ specimens. Longitudinal macro-buckling of the specimen is shown in Figure 2. A failure mode typically not observed in MMCs, i.e. delamination, was also observed. Premature buckling may not allow evaluation of proper mechanical response and properties at higher stress or strains. Therefore, lateral restraint for unidirectional higher strength MMCs are essential to develop a good understanding of key deformation mechanisms under pure compressive loading.

Following mechanical testing, most of the compression specimens were not loaded to failure. A number of specimens were polished at the edges. A fairly complex polishing procedure has been developed at Battelle for evaluating MMCs to preserve the characteristics

of deformation. Repeated polishing was performed on a few tested and untested samples to confirm that any cracking, debonding, or slip bands was due to deformation alone, and not associated with the polishing procedure or manufacturing. Specimens were etched using Kroll's reagent, which was found to be effective in revealing slip bands both at surface and subsurface locations. Metallographic specimens were examined optically and key deformation characteristics were photographed.

The overall test matrix is given in Table 1. The study did not allow for any statistical property evaluation.

RESULTS AND DISCUSSION

Mechanical Behavior Evaluation

Longitudinal Lamina

The typical stress-strain response including unloading for a $[0]_8$ specimen is shown in Figure 3. The compression test result without buckling guides is also shown in the same figure. The elastic modulus in tension and compression were similar, ranging between 175-179 GPa. Also, the corresponding tension data is presented in the same plot. It may be noted that the compression capability of the $[0]_8$ lamina is significantly higher than the tension case both in terms of (1) the onset of nonlinearity and (2) the higher ultimate strength (when premature buckling is avoided). The compression specimen was not loaded to failure. However, experimental efforts suggest that the compression strength will be quite high. In the absence of restraint for buckling, it is clear that premature buckling takes place resulting in no useful information in the nonlinear deformation regime. The failure mode for compression without buckling guides will be discussed in the Microstructural Evaluation section. The unloading line is parallel to the elastic loading line for the $[0]_8$ composite and indicate that the deformation response is controlled primarily by plastic deformation. The mechanical responses at 538 C and 650 C are included in Figure 4 along with room temperature response. Table 2 provides data on the effect of temperature on the proportional

limit and modulus. The decrease in modulus and proportional limit are due to the decrease in flow properties of the matrix at elevated temperature.

The onset of non-linear deformation at RT in compression (approx. 2200 MPa) was significantly higher than in tension (approx. 980 MPa). This difference is due to a residual tensile stress in the matrix; calculations show [11] that for this system the axial residual stresses at room temperature (RT) are approximately 412 MPa in the matrix at the fiber-matrix interface, and -1000 MPa in the fiber. Assuming an elastic one-dimensional response, the residual axial stress can be calculated using the formula $S_r = [(|S_c| - |S_t|)/2)*E_m/E_c$, where S_c and S_t are the measured proportional limits in compression and tension, and E_m and E_c are matrix and composite moduli. Using this formula, the tensile axial residual stress in the matrix is calculated to be 335 MPa.

Transverse Lamina

Figure 5 shows the typical stress-strain response of the $[90]_8$ lamina for the three different temperatures, namely, room temperature, 538°C (1000°F) and 650°C (1200°F). In each case, the specimens were unloaded in the nonlinear regime. There is a progressive loss in elastic modulus and proportional limit as a function of temperature as given in Table 3. The distinct knee observed in tension for the onset of nonlinearity in the $[90]_8$ lamina (Figure 5) is clearly absent in the case of compression. The onset of nonlinearity in the tension stress-strain curve was attributed to fiber-matrix debonding - a dominant damage mechanism for the $[90]_8$ MMC lamina. Note the large work hardening period for the MMC, extending from approximately 0.5 percent strain to approximately 1 percent strain. This period was much longer then for the matrix material.

The room temperature and 538°C compression stress-strain results are compared in Figure 6 with those of the tension case to accentuate the difference in the response of the same SCS-6/Ti 15-3 composites under different loading conditions. This plot also contains the pure matrix stress-strain response in tension at room temperature and at 538°C. There are two important observations that can be made from this comparison; 1) the initial elastic or tangent moduli under tension and compression are similar, and 2) the proportional limits

in compression are higher than for their corresponding tension counterparts. The higher proportional limit can be explained by the presence of a beneficial tensile residual stress which must be overcome in compression before a compressive proportional limit is reached. A matrix average radial residual compressive stress of ~ 190 MPa at room temperature, estimated from the proportional limits in tension and compression, compares well with a prediction of ~ 200 MPa using Finite Element Analysis (FEA).

The unloading characteristics for the $[90]_8$ specimens under compression are quite different than those observed in tension. The initial unloading line is parallel to the initial loading line in compression signifying plastic deformation at work. The offset strains in each case for all temperatures is significantly large (Figure 5). Further unloading results in a somewhat more compliant behavior as zero load is approached.

Microstructural Evaluation

Longitudinal Lamina

Optical photomicrographs of replicas taken from polished specimens show the presence of extensive matrix plasticity in the lamina (Figure 7). Fiber-matrix debonding is also evident at higher strain levels within the ply. These observations were only made at room temperature. The failure due to fiber buckling in an unrestrained test is shown in Figure 8. The fibers break in a shear plane within the gage section. This failure is indicative of a buckling instability due to compressive load.

Transverse Lamina

Optical photomicrographs of specimens polished after testing revealed the nature of deformation characteristics under compressive loading quite clearly. The initial deformation mechanism under monotonic compressive loading is found to be matrix plasticity along the loading axis between fibers as shown in Figure 9 for a specimen tested at room temperature. This appears to be a dominant mechanism controlled by high strains between the fibers

within a ply along the loading line during compression and less plasticity between the adjacent plies. This partitioning of plasticity likely was responsible for the high work hardening that were observed for the compression specimen (Figure 6). It may be recalled that in the case of tension, there was only a knee associated with debonding and the smooth behavior under compression as shown in Figure 6 was absent. The slip lines are considerably more prominent compared to the similar slip lines observed in the tension case at similar locations [7,9]. In the case of tension, the initial micro-plasticity is followed by fiber-matrix debonding at the fiber poles at the onset of departure from the linear elastic response (knee). In the case of compression, the nonlinearity is a smooth one (Figure 6) without any abrupt change from linearity. Debonding, as observed in the tension case at the two poles of a fiber, is absent in the compression case, as the matrix is in compression at the poles of the fiber (top and bottom points on the fibers in Figure 9).

Careful observation also reveals a very interesting damage condition in the composite under compression. There are radial cracks within the fibers oriented primarily along the compression loading axis which form after the initial slip lines have developed in the matrix as mentioned earlier. Reaction zone cracks (RZC) are also observed. These damage modes are depicted in Figure 10. This damage mode was reported earlier by Newaz and Majumdar [12-14]. Radial fiber cracking is indicative of the low radial fiber strength which may be related to the soft carbon core in the SCS-6 fiber and the columnar grain structure of the CVD deposited SiC with grain boundary facets oriented radially. These cracks are not observed in as-received materials and were not observed in the tension loading mode.

In the nonlinear regime, further compressive deformation of the composite results in the development of bulk plasticity in the matrix with extensive networks of shear slip bands. This is illustrated in the Figures 11a and 11b for specimens tested at 538°C and 650°C. These micrographs were taken under polarized light to capture the active slip bands. Also, it may be noted that there is significant debonding of fiber and matrix at 90-degree locations from the loading axis. This is in contrast to the debonding at the poles for the tension case. This is clearly shown in Figures 12a and 12b. Qualitatively, the debonding in compression can be attributed to high local tensile transverse strains at the fiber-matrix interface which develop during compressive deformation of the specimen. Shear strains at the fiber-matrix

interface are also expected. However, precise computational analysis will be required to determine the contribution of normal and shear strains to the debonding phenomena observed.

The transverse compression response is compared with the transverse tension response in Table 4 in terms of the leading inelastic deformation mechanisms. Although, the radial cracking of fiber in compression is a concern, it may be noted that the most debilitating damage, i.e. one that occurs at a fairly low strain level, is fiber-matrix debonding under tension. Radial fiber cracking is observed in compression at a strain level of 0.007 whereas debonding under tension initiates around a strain level of 0.003.

The sequence and location of damage development under tension and compression can explain the different stress-strain responses of the composite. Furthermore, this specific behavior with regard to the "knee" can be rationalized based on the effect of debonding orientation on the mechanical response of the composites in tension and compression as illustrated in Figure 18. Reaction zone cracks and debonding which are perpendicular to load axis as in the case in tension are anticipated to have a larger effect on compliance.

ANALYTICAL CONSIDERATIONS

Within the scope of the compression investigation, an effort was made to determine the suitability of a few constitutive models to predict the stress-strain response under monotonic compression. Our effort was only confined to the transverse constitutive response.

A unique set of micromechanics equations have been developed by NASA researchers for high temperature metal matrix composites [15]. These equations coupled with a set of thermoviscoplastic nonlinear multifactor relations developed by these researchers [16] are consolidated into a computational code titled METCAN. It treats the material nonlinearity at the constituent level, where the material's non-linear time-temperature-stress dependence is modeled using power-law type multifactor interaction relationships. Although the model can account for interface damage in a limited way, by changing the mechanical properties of the interphase region (the region consisting of the reaction-zone and the interfaces), it cannot predict a priori what the interphase property should be. METCAN was used to predict the

stress-strain behavior for both $[0]_8$ and $[90]_8$ SCS-6/Ti 15-3 laminae under both room and elevated temperature. These results are presented in Figures 13a and 13b. The correlations are quite good and are encouraging. METCAN is not suitable for unloading and therefore, no attempt was made to predict the unloading response.

Also, the AGLPLY code was used (continuum plasticity based model by Dvorak and Baheiel-Din [17]) which is based on a vanishing fiber diameter model, and can be used effectively to predict lamina and laminate responses from the elastic-plastic responses of the matrix and fiber materials. The primary drawback of the model is that it cannot account for damage. Comparison of the AGLPLY predictions with experimental data for the $[0]_8$ MMC at room temperature is given in Figure 14. In the predictions, the $[90]_8$ MMC are compared with experimental data in Figure 15. The figure also includes experimental data obtained by Lerch [18] at NASA Lewis using a 32-ply MMC without any buckling guides. While the experimental data from the two investigations are in agreement, the AGLPLY predictions are not good in the inelastic regime of deformation. Rather, AGLPLY appeared to mimic the matrix behavior. The inadequacy of AGLPLY prediction may be related to the assumption of vanishing fiber diameter which averages out the microstructure and cannot account for the way plasticity is partitioned between different regions of the MMC.

Battelle's finite element computational unit cell model developed by Brust, et al. [11] was also used to predict the stress-strain response of $[0]_8$ and $[90]_8$ laminae for the room temperature case. The following analytical aspects were involved in the model: (1) 2-D generalized plane-strain conditions, (2) periodic boundary conditions, (3) classical thermal plasticity for the matrix, whose property was assumed to be independent of position, (4) thermo-elastic properties of the fiber, and (5) the fiber-matrix interface was modeled as a discrete interface. For the case of simulating constraints due to the buckling guides, transverse stiffening was modeled using springs with appropriate constants. The results are shown in Figures 16 and 17. The correlation of experimental and predicted results are quite good. Notably, the unloading response was captured for the more complex $[90]_8$ stress-strain response. The compliance change late in unloading at low loads requires further clarification. This work is currently underway at Battelle.

CONCLUSIONS

Based on the current investigation, the following conclusions can be reached.

1. Inelastic deformation in the $[0]_8$ lamina under compression is controlled primarily by matrix plasticity. Some fiber-matrix debonding is also observed.

2. Premature buckling can result if restraints (buckling guides) are not used for $[0]_8$ lamina in compression.

3. Macroscopic instability resulting in fiber failure by buckling within a shear zone in the gage section of the specimen was observed in longitudinal compression for the $[0]_8$ lamina.

4. The mechanical response and deformation characteristics in SCS-6/Ti 15-3 $[90]_8$ lamina are different in monotonic tension and compression. The characteristic early knee associated with fiber-matrix debonding in the stress-strain response of the $[90]_8$ lamina under tension is absent in the case of the monotonic compressive response.

5. There is a marked decrease in proportional limit and increased ductility as the temperature is increased for both the $[0]_8$ and the $[90]_8$ SCS-6/Ti 15-3 laminae in compression. These can be rationalized in terms of matrix flow properties.

6. Radial fiber fracture at the carbon core in SCS-6 fibers is a distinct damage mechanism observed under compressive loading in the $[90]_8$ lamina. The transverse compression capability of the SCS-6 fibers are anticipated to be low due to the columnar structure of the SCS-6 fiber. Extensive matrix plasticity and debonding are also dominant mechanisms under compression. These mechanisms are observed at elevated temperature as well.

7. AGLPLY analysis predicts the $[0]_8$ stress-strain response quite well, but does not predict the $[90]_8$ response as well. Also, computational results using NASA's METCAN and Battelle's Unit Cell Model adequately predict the stress-strain response of both the $[0]_8$ and $[90]_8$ laminae under compression.

ACKNOWLEDGEMENT

This work was part of a continuing HITEMP program sponsored by NASA-LeRC under Contract #NAS3-26494. This program was monitored by Dr. B. A. Lerch. Encouragement and interaction of Dr. B. A. Lerch, Dr. J. R. Ellis and Dr. Steve Arnold of NASA-LeRC are acknowledged. Mr. Norm Frey and Mr. Glenn Foster of Battelle are recognized for their excellent efforts in testing and in microscopy. Dr. F. W. Brust and Mr. S. Naboulsi from Battelle are acknowledged for the computational results. Dr. S. Mital of University of Toledo is thanked for the METCAN results.

REFERENCES

1. Sun, C. T., "Modeling Continuous Fiber Metal Matrix Composite as an Orthotropic Elastic-Plastic Material", ASTM STP 1032, 1989, pp. 148-160.

2. Lerch, B. A. and Saltsman, J. F., "Tensile Deformation Damage in SiC Reinforced Ti-15V-3Cr-3Al-3Sn", NASA Technical Memorandum 103620, April, 1991.

3. Majumdar, B. S. and Newaz, G. M., "Thermomechanical Fatigue of a Quasi-Isotropic Metal Matrix Composite", ASTM STP 1110, 1991, pp. 732-752.

4. Newaz, G. M., Majumdar, B. S. and Brust, F. W., "Thermal Cycling Response of Quasi-Isotropic Metal-Matrix Composites", ASME J. of Engg. Materials and Technology, April, 1992, pp. 156-161.

5. Johnson, W. S., Lubowinski, S. J. and Highsmith, A. L., "Mechanical Characterization of Unnotched SCS-6/Ti-15-3 Metal Matrix Composites at Room Temperature", ASTM STP 1080, pp. 193-218, 1990.

6. Nimmer, R. P., Bankert, R. J., Russell, E. S., Smith, G. A. and Wright, K. P., "Micromechanical Modeling of Fiber/ Matrix Interface Effects in Transversely Loaded SiC/Ti-6-4 Metal Matrix Composites Technology and Research, Vol. 13, #1, 1991, pp. 3-13.

7. Majumdar, B. S. and Newaz, G. M., "Inelastic Deformation in Metal Matrix Composites: Plasticity and Damage Mechanisms", Philosophical Magazine, London, 1992, Vol. 66, #2, pp 187-212.

8. Gunawardena, S. R., Jansson, S. and Leckie, F. A., "Transverse Ductilities of Metal Matrix Composites", AD-22, ASME Winter Annual Meeting, Atlanta, December, 1991, pp. 23-30.

9. Newaz, G. M. and Majumdar, B. S., "Deformation and Failure Mechanisms in MMC", AD-22, ASME Winter Annual Meeting, Atlanta, 1991, pp. 55-66.

10. Lamothe, R. M. and Nunes, J., "Evaluation of Fixturing for Compression Testing of Metal Matrix and Polymer Matrix Composites", ASTM STP 808, R. Chait and R. Paprino, Eds., 1983, pp. 241-253.

11. Brust, F. W., Majumdar, B. S., and Newaz, G. M., "Constitutive and Damage Response of Ti 15-3/SCS-6 MMC," presented at the ASTM Conference on Fatigue and Fracture, Pittsburgh, PA, (May 4-5, 1992).

12. Newaz, G. M. and Majumdar, B. S., "Failure Modes in Transverse MMC Lamina Under Compression" accepted for publication in the J. of Materials Science & Letters, UK, December, 1992.

13. Newaz, G. M. and Majumdar, B. S., "Inelastic Deformation Mechanisms in a Transverse MMC Lamina Under Compression," AD-Vol. 27, Fracture and Damage, ASME Winter Annual Meeting, Anaheim, 1992, pp. 77-84.

14. Majumdar, B. S. and Newaz, G. M., "Inelastic Deformation Mechanisms in MMC: Compression and Fatigue," HITEMP Review, NASA Conference Publication 10104, 1992, p. 49-1.

15. Hopkins, D. A. and Chamis, C. C., "A Unique Set of Micromechanics Equations for High-Temperature Metal Matrix Composites," ASTM STP 964, 1988, pp. 159-176.

16. Chamis, C. L. and Hopkins, D. A., "Thermoviscoplastic Nonlinear Constitutive Relationships for Structural Analysis of High-Temperature Metal Matrix Composites," ASTM STP 964, 1988, pp. 177-196.

17. Dvorak, G. J. and Bahei-El-Din, Y. A., J. Applied Mechanics, Vol. 49, 1982, pp. 327-335.

18. Lerch, B. A. Private communication, NASA-LeRC, Cleveland, December, 1992.

TABLE 1. COMPRESSION TEST MATRIX
(SCS-6/Ti 15-3)

Layup	Number of Specimens	Temperature	Comments
$[0]_8$	1	RT	Stress-strain, edge replication
	2	RT	Intermediate unloading
	1	RT	Without guides
	1	538 C	Stress-strain, unloading
	1	650 C	Stress-strain, unloading
$[90]_8$	1	RT	Stress-strain
	2	RT	Intermediate unloading
	1	RT	Edge replication
	1	538 C	Stress-strain, unloading
	1	650 C	Stress-strain, unloading

TABLE 2. $[0]_8$ SCS-6/Ti 15-3 PROPERTIES IN COMPRESSION

Temperature	Young's Modulus (GPa)	Proportional Limit	
		Stress (MPa)	Strain
RT	179	2200	0.012
538 C	170	1200	0.007
650 C	150	600	0.004

TABLE 3. $[90]_8$ SCS-6/Ti 15-3 PROPERTIES IN COMPRESSION

Temperature	Young's Modulus (GPa)	Proportional Limit	
		Stress (MPa)	Strain
RT	125	697	0.006
538 C	108	428	0.004
650 C	92	276	0.003

TABLE 4. DEFORMATION MECHANISMS IN TENSION AND COMPRESSION

$[90]_8$ SCS-6/Ti 15-3				
	Tension		Compression	
Inelastic Deformation Mechanisms	Strain	Stress, MPa	Strain	Stress, MPa
Plastic Slip Band	0.002	225	0.002*	225*
Debonding	0.003-0.005	280-340	0.006-0.008	700-900
Reaction Zone Cracks	0.005	350	0.006	700
Radial Fiber Cracking	--	--	0.006-0.008	700-900
Extensive Matrix Plasticity	>0.006	400	>0.01	900

* data not retrievable at earlier strain/stress levels because of loss of replica

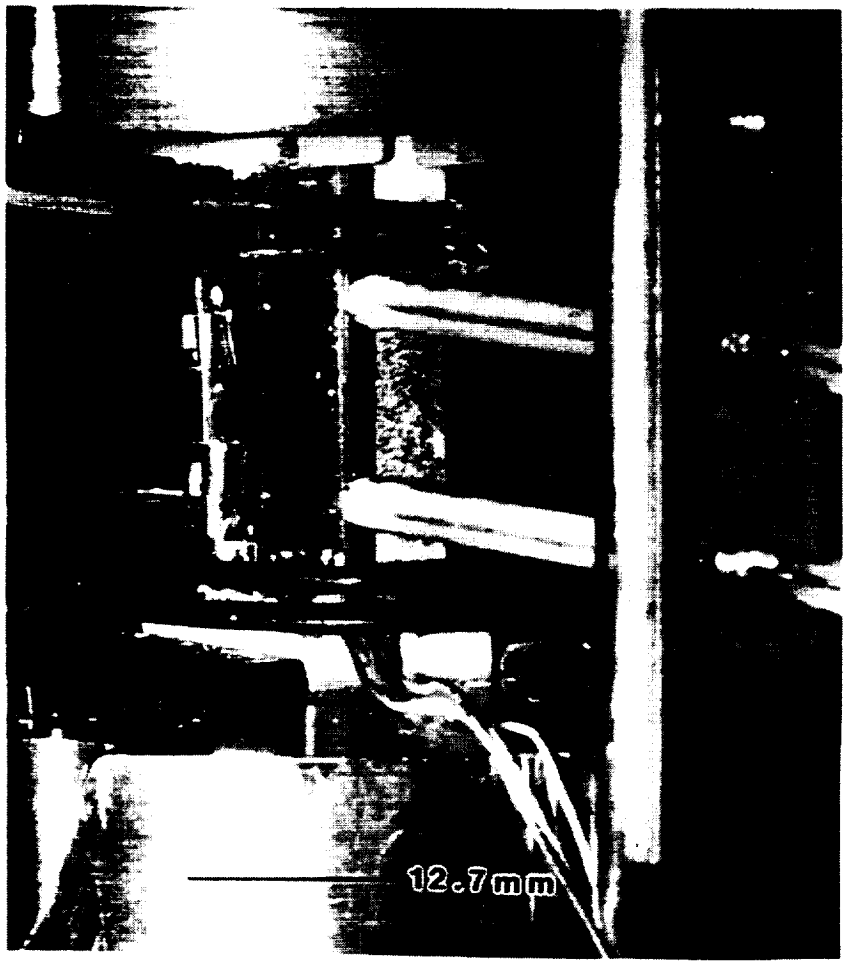

FIGURE 1. COMPRESSION TEST SETUP

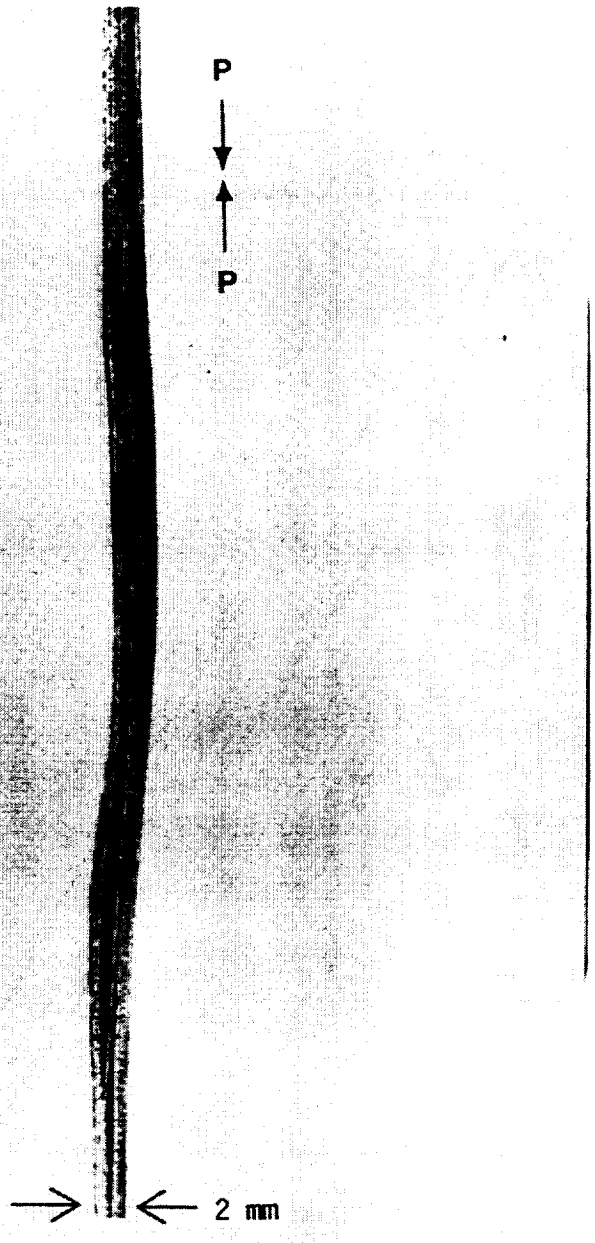

FIGURE 2. MACROBUCKLING OF UNIDIRECTIONAL SPECIMEN WITHOUT RESTRAINTS, SUBJECTED TO COMPRESSION.

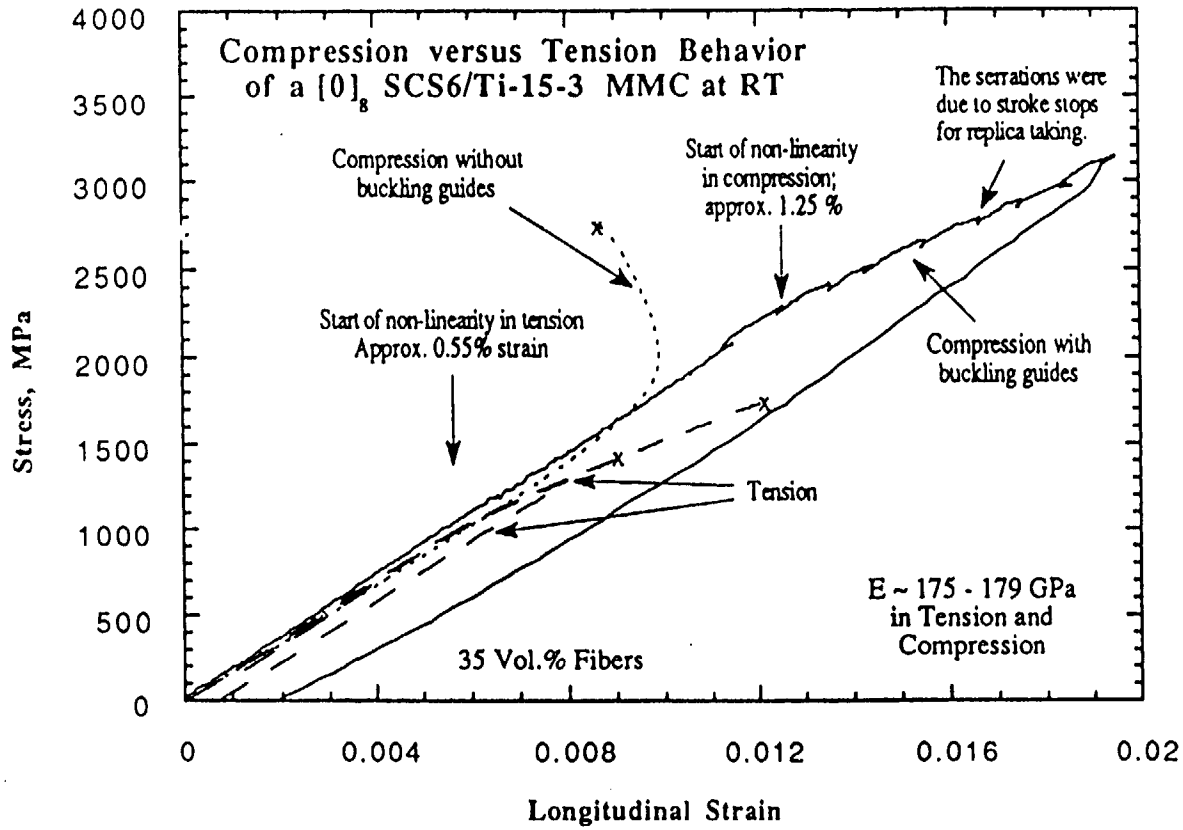

FIGURE 3. TYPICAL STRESS-STRAIN RESPONSE OF $[0]_8$ LAMINA IN COMPRESSION. ALSO INCLUDES TENSION RESULTS FOR THE SAME LAMINA.

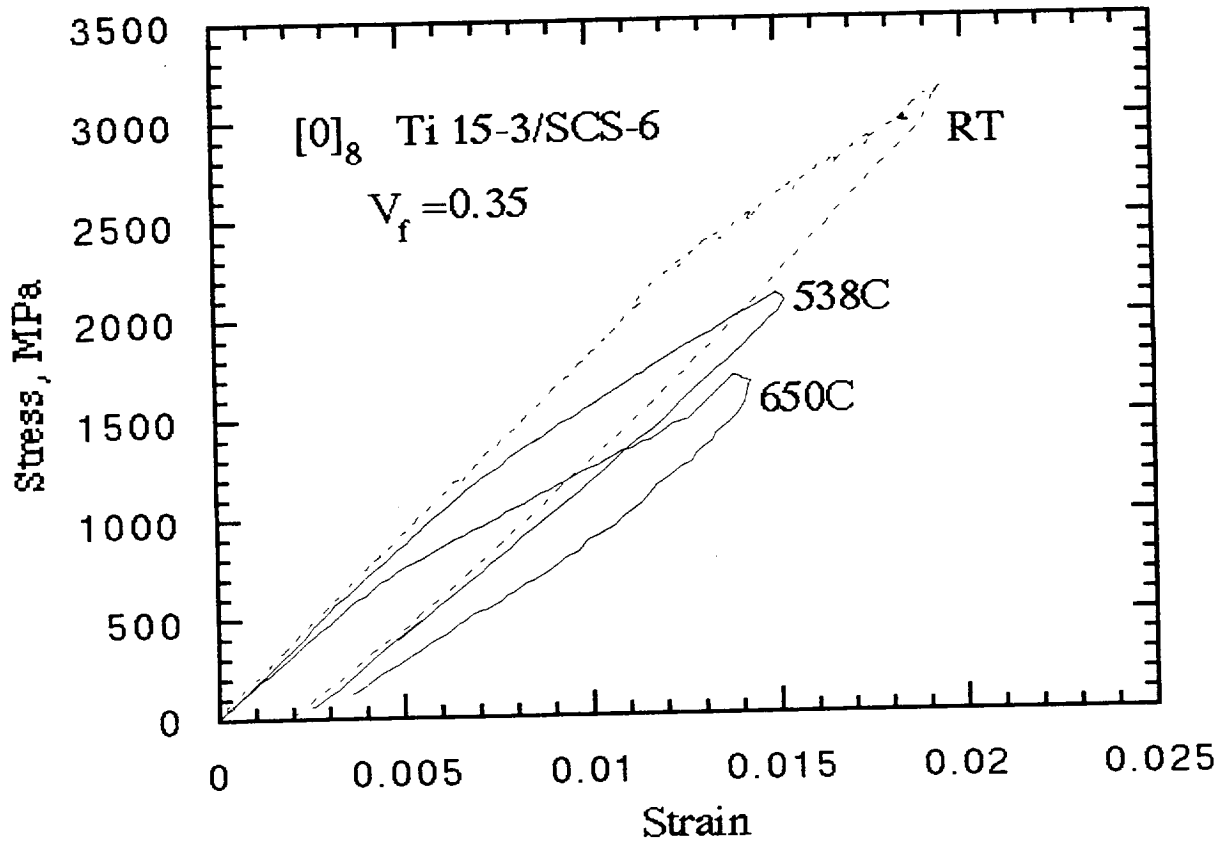

FIGURE 4. MECHANICAL RESPONSE AT ELEVATED TEMPERATURE FOR $[0]_8$ LAMINA IN COMPRESSION

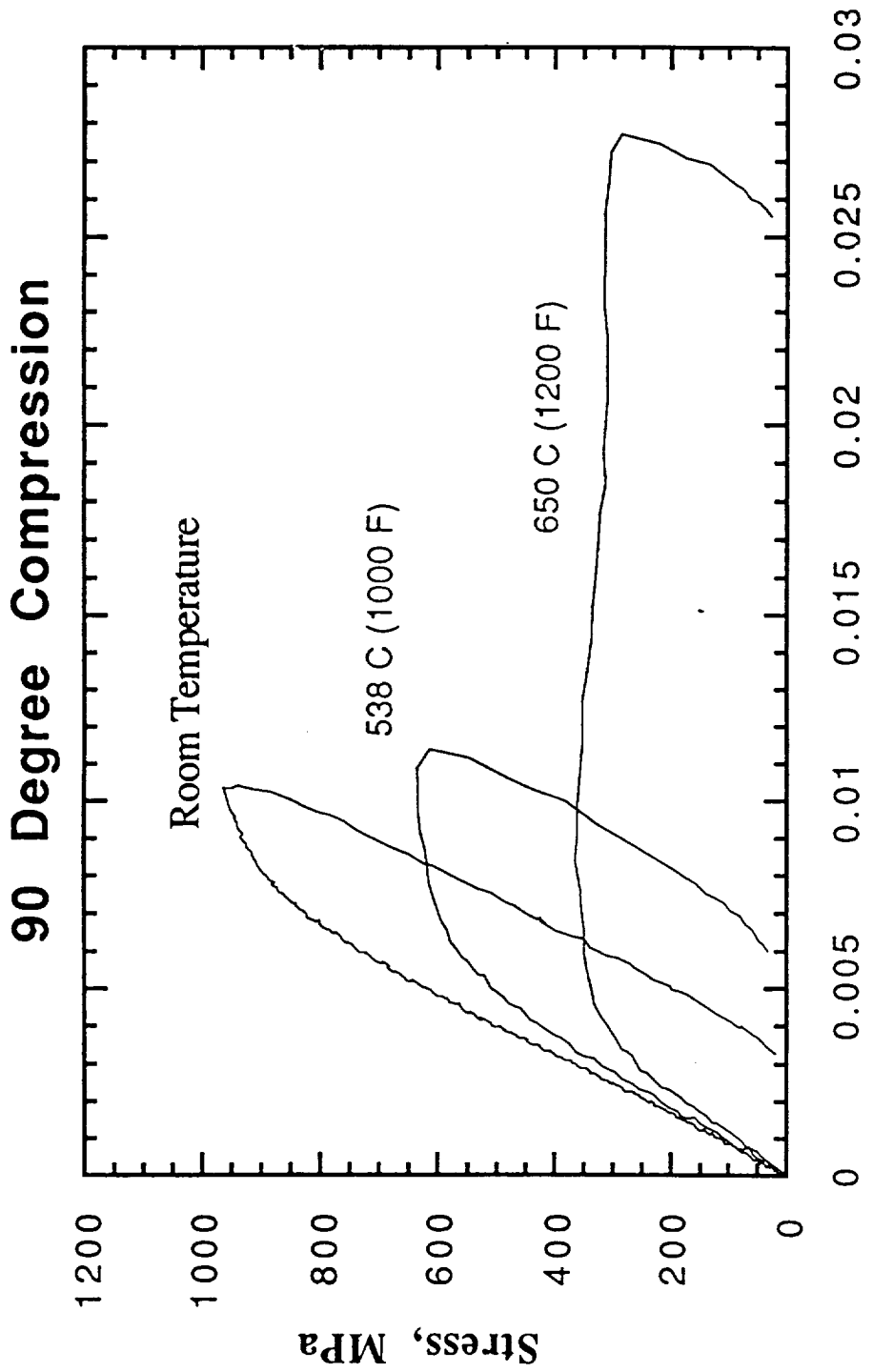

FIGURE 5. MECHANICAL RESPONSE OF $[90]_8$ LAMINA IN COMPRESSION

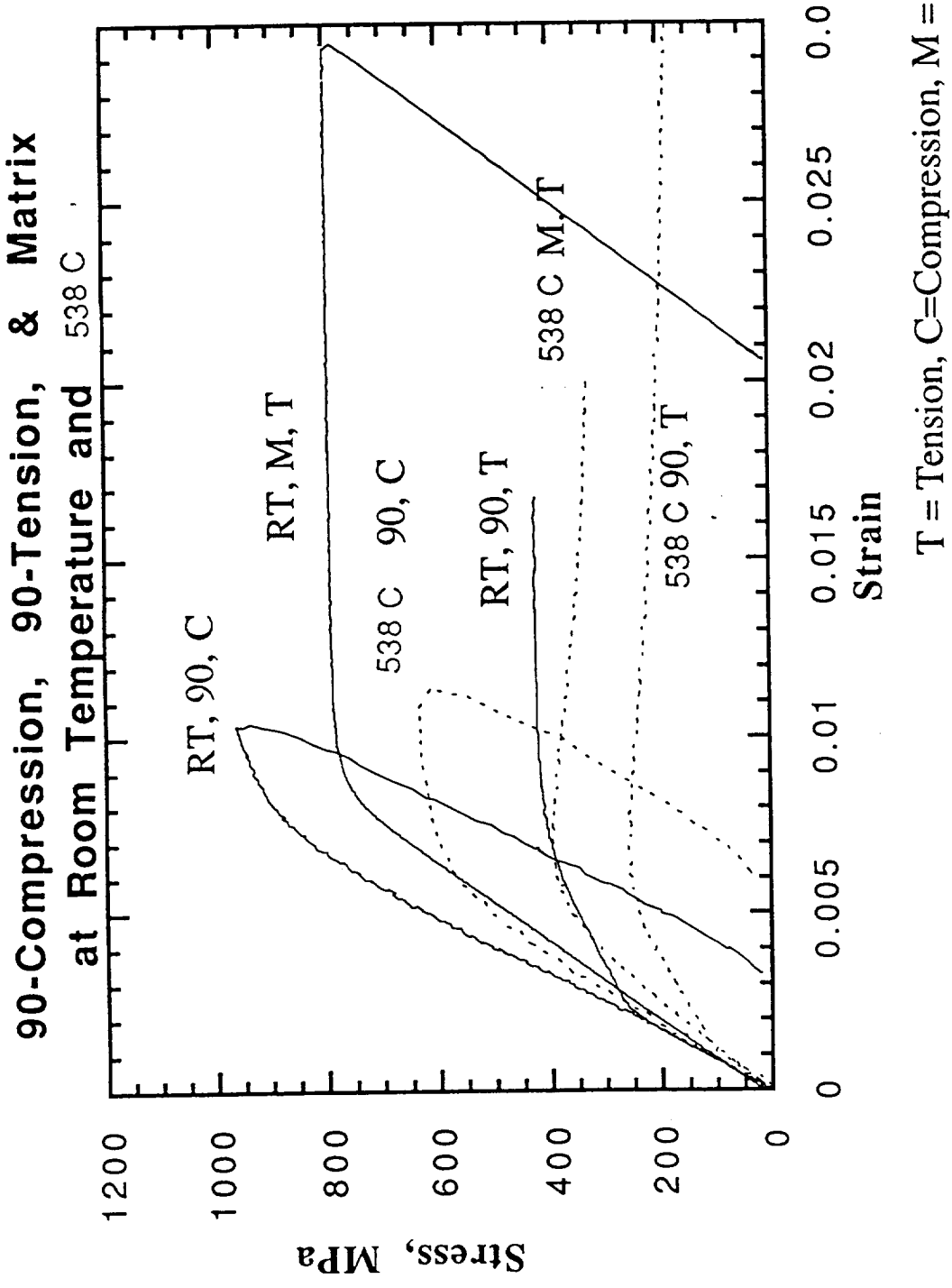

FIGURE 6. COMPARISON OF COMPRESSION AND TENSION RESPONSE OF $[90]_8$ LAMINA. MATRIX BEHAVIOR IN TENSION IS SHOWN TOO.

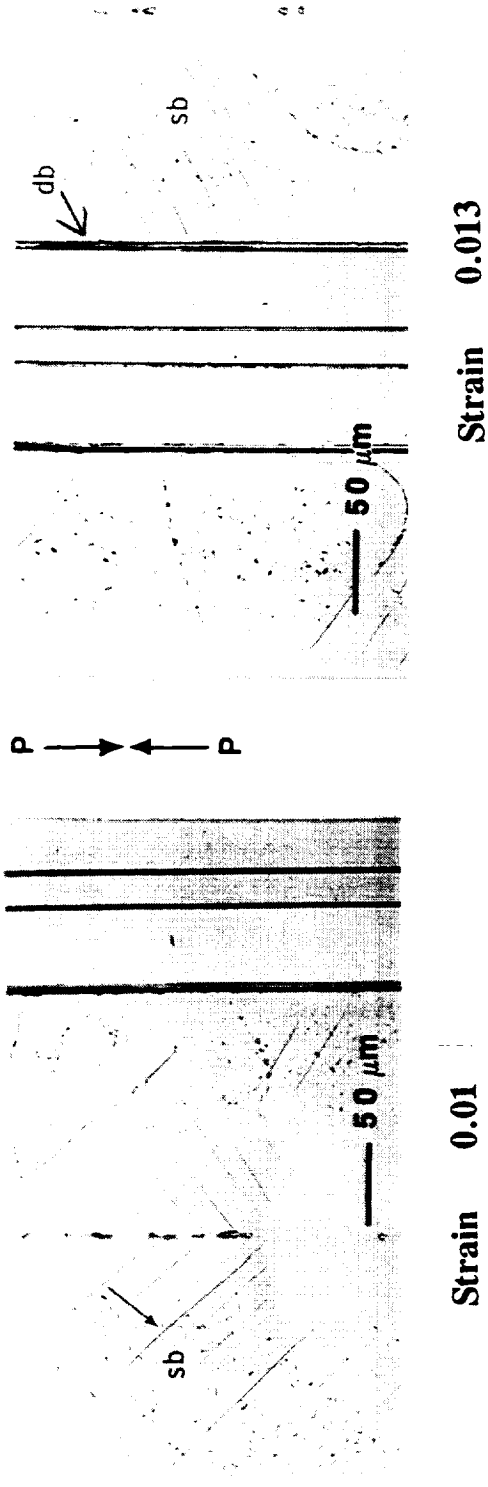

FIGURE 7. PLASTIC SLIP BANDS (sb) AND DEBONDING (db) IN $[0]_8$ LAMINA AT RT IN COMPRESSION.

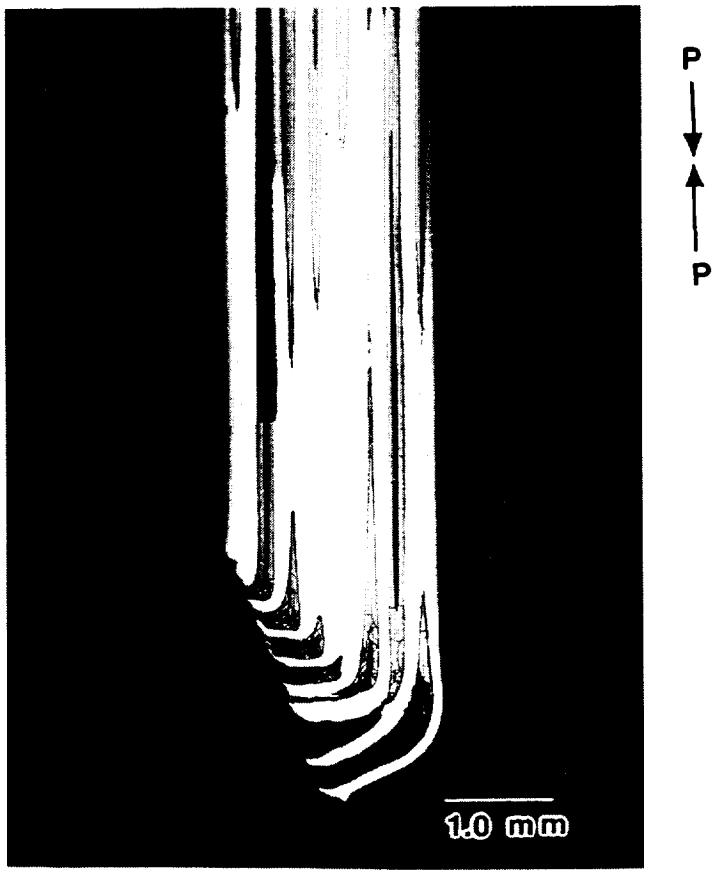

FIGURE 8. FIBER BUCKLING IN $[0]_8$ LAMINA IN COMPRESSION AT RT.

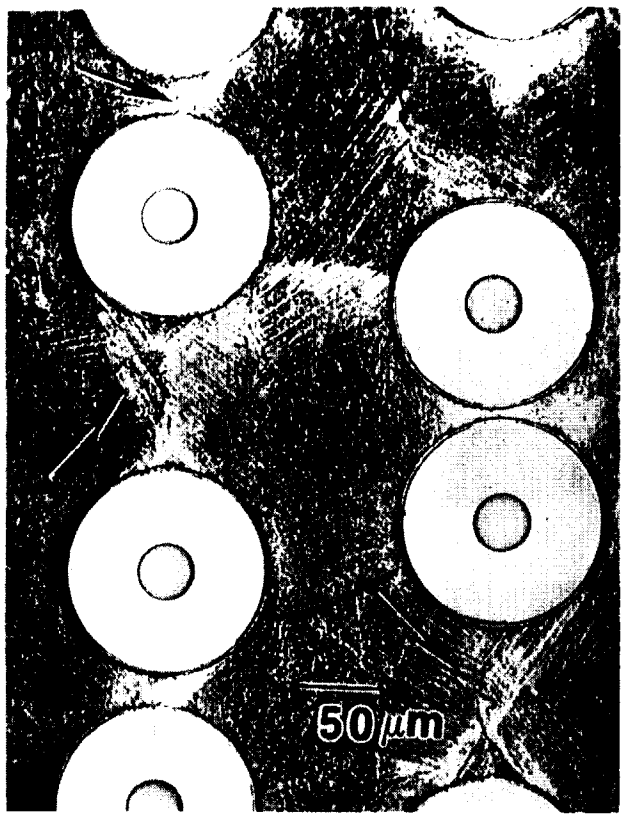

FIGURE 9. MATRIX PLASTICITY BETWEEN FIBERS IN Ti 15-3/SCS-6 $[90]_8$ LAMINA UNDER COMPRESSION AT ROOM TEMPERATURE. LOADING IS UP AND DOWN.

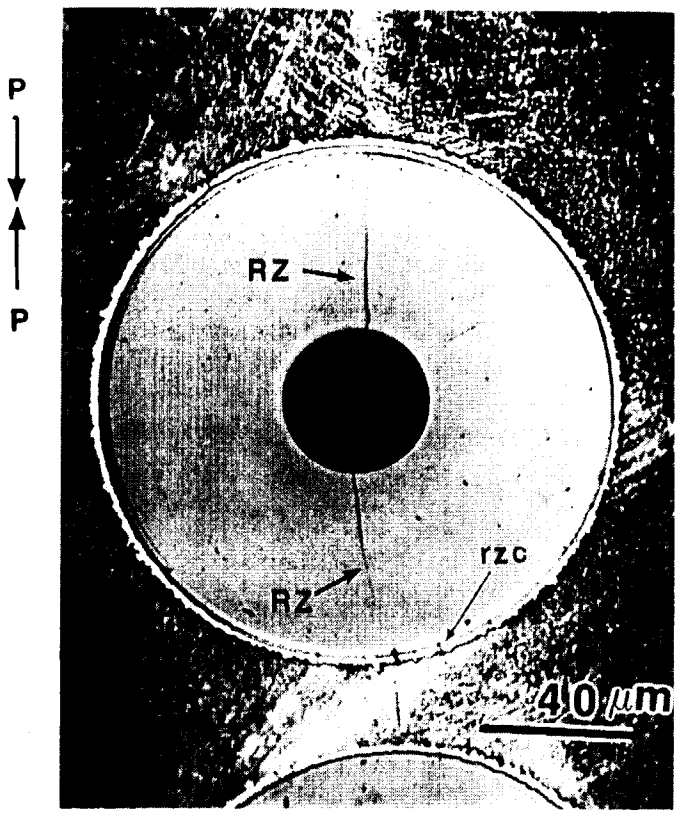

FIGURE 10. RADIAL CRACKS IN SCS-6 FIBER IN A $[90]_8$ Ti 15-3/SCS-6, LAMINA UNDER COMPRESSION AT ROOM TEMPERATURE. LOADING IS UP AND DOWN.

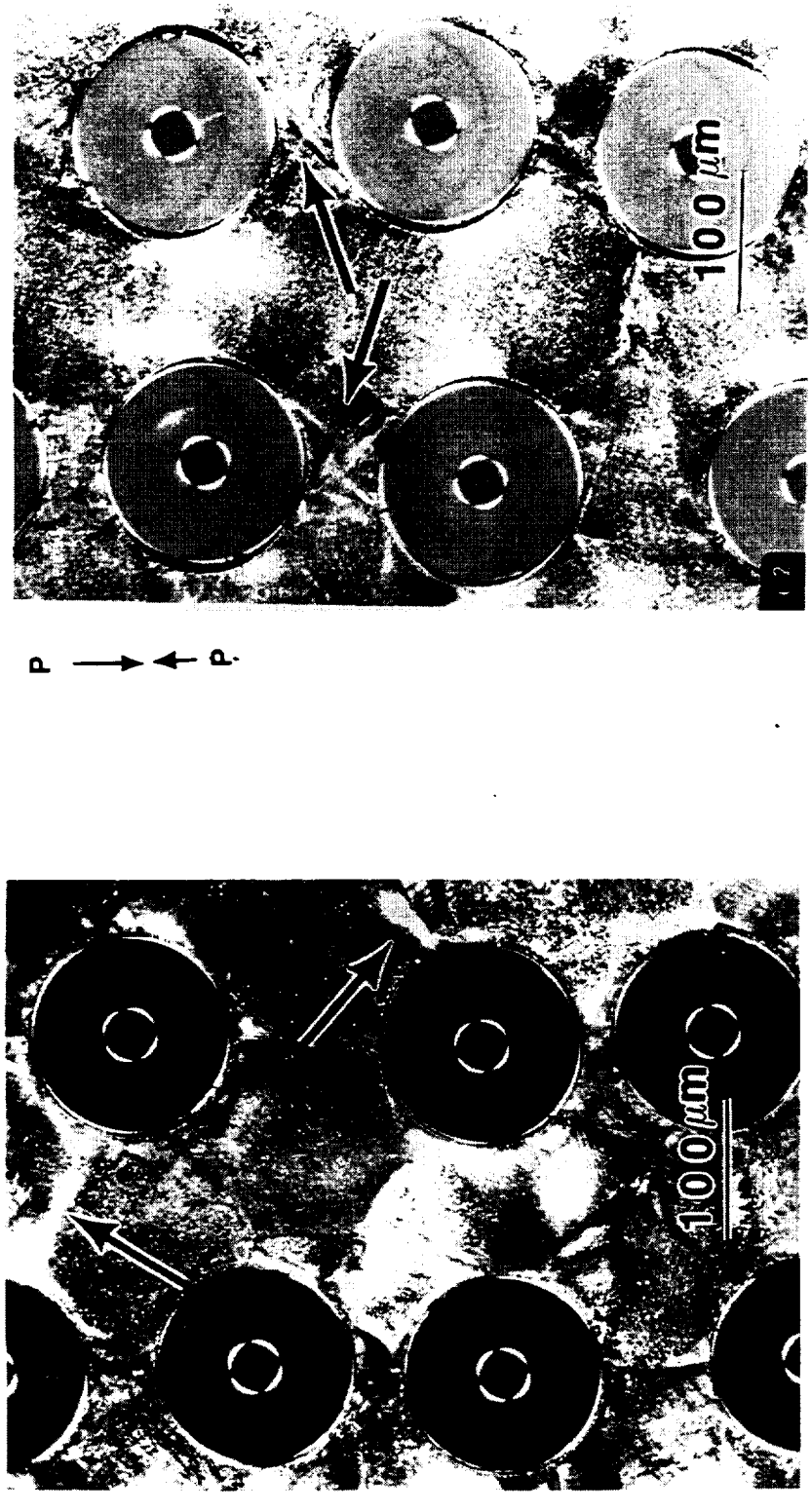

FIGURE 11. MATRIX PLASTICITY IN THE FORM OF CONCENTRATED SHEAR SLIP BANDS IN $[90]_8$ Ti 15-3/SCS-6 LAMINA UNDER COMPRESSION AT a) 538°C and b) 650°C.

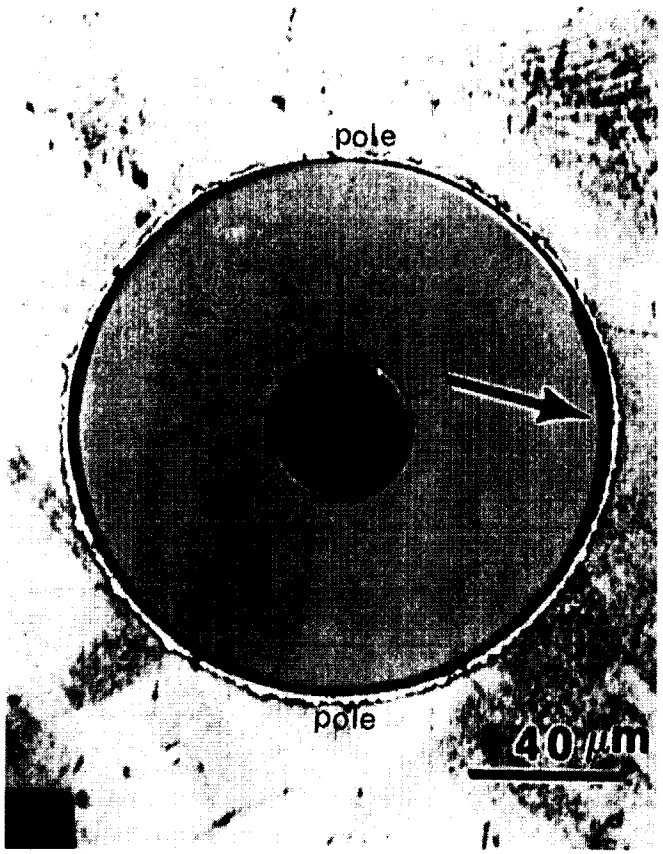

a) 538°C

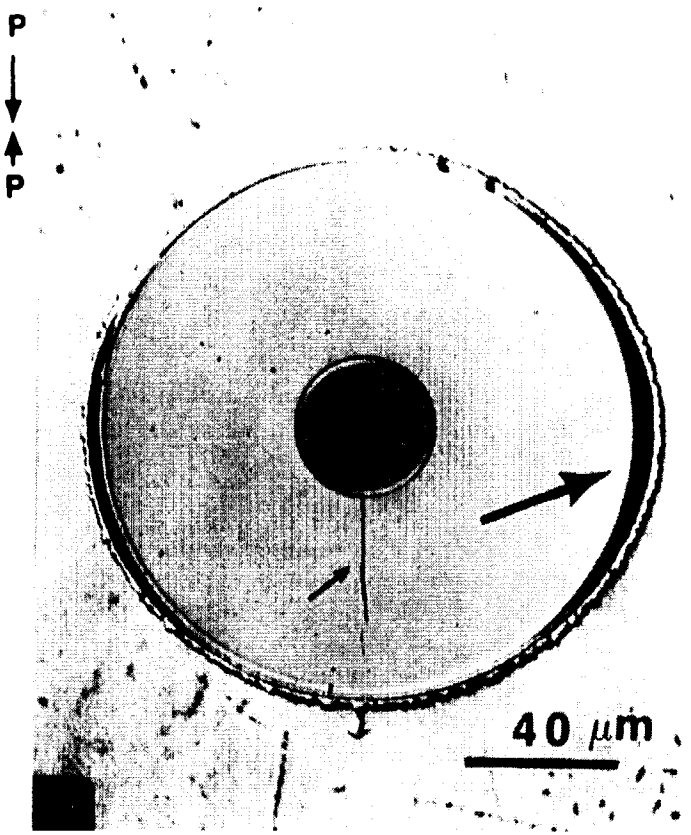

b) 650°C

FIGURE 12. DEBONDING (LARGE ARROW) AND RADIAL FIBER CRACKING (SMALL ARROW) IN $[90]_8$ Ti 15-3/SCS-6 LAMINA AT a) 538°C AND b) 650°C LOADING IS UP AND DOWN

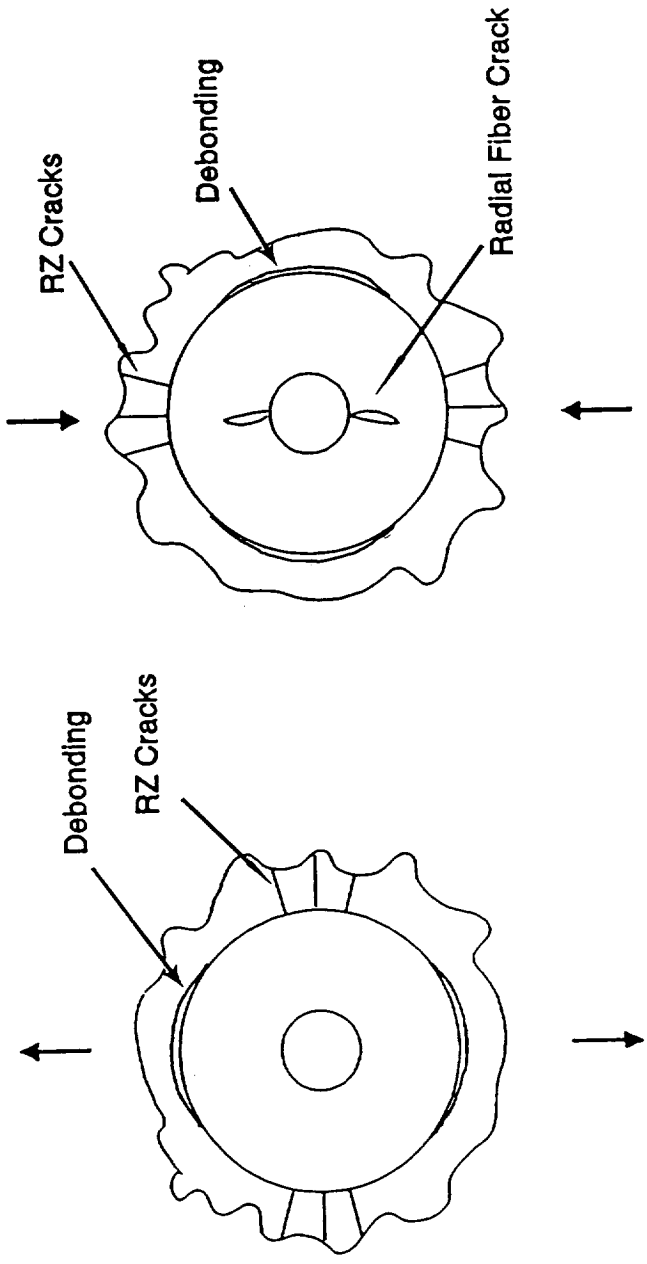

FIGURE 13. ORIENTATION OF DAMAGE (CRACKING) IN TENSION AND COMPRESSION

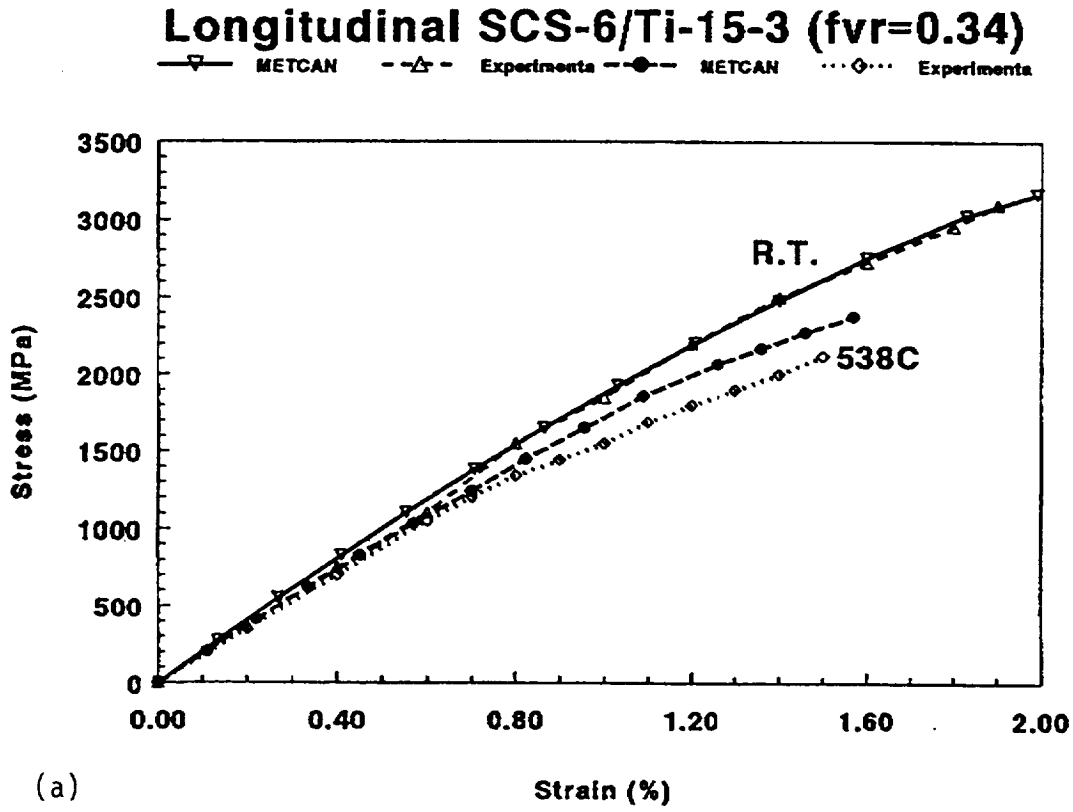

(a)

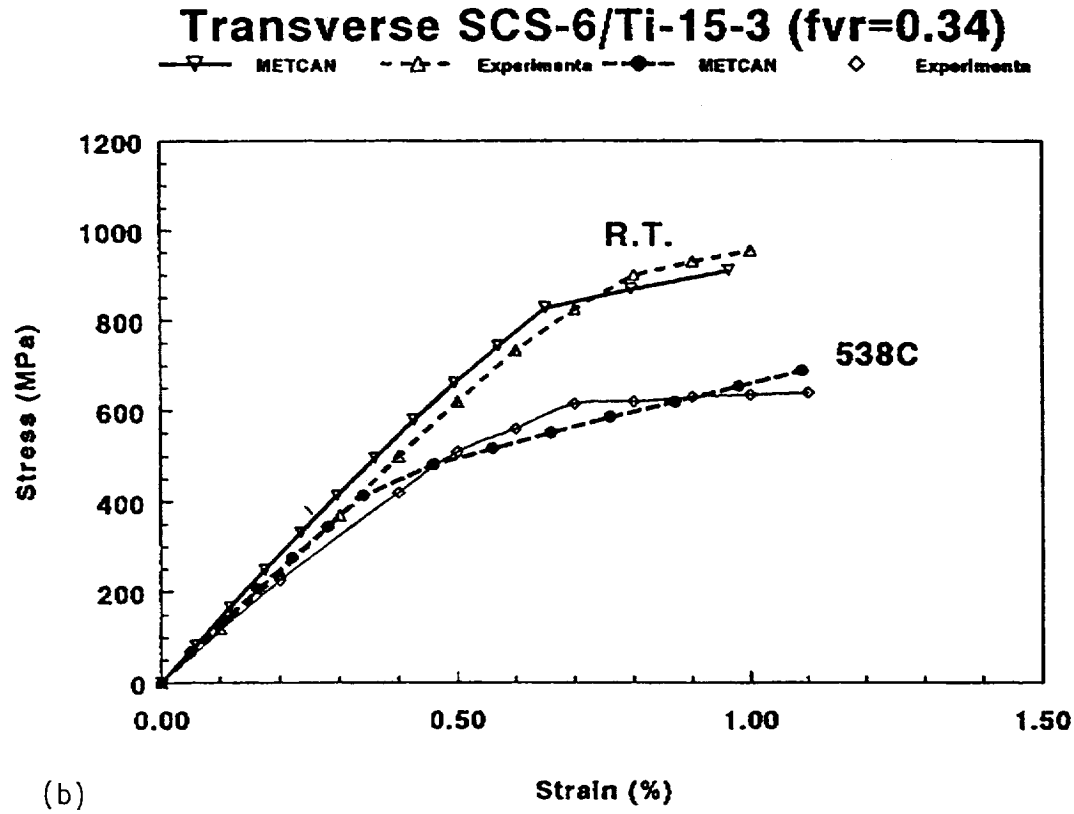

(b)

FIGURE 14. METCAN ANALYSIS RESULTS FOR a) $[0]_8$ and b) $[90]_8$ STRESS-STRAIN RESPONSE IN COMPRESSION

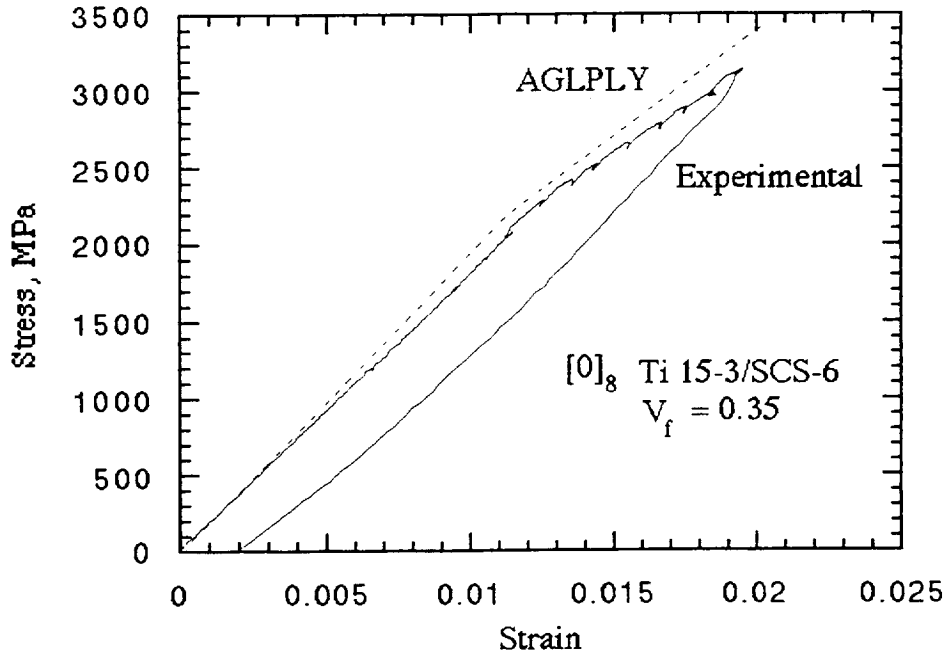

FIGURE 15. AGLPLY ANALYSIS RESULTS FOR $[0]_8$ STRESS-STRAIN RESPONSE IN COMPRESSION

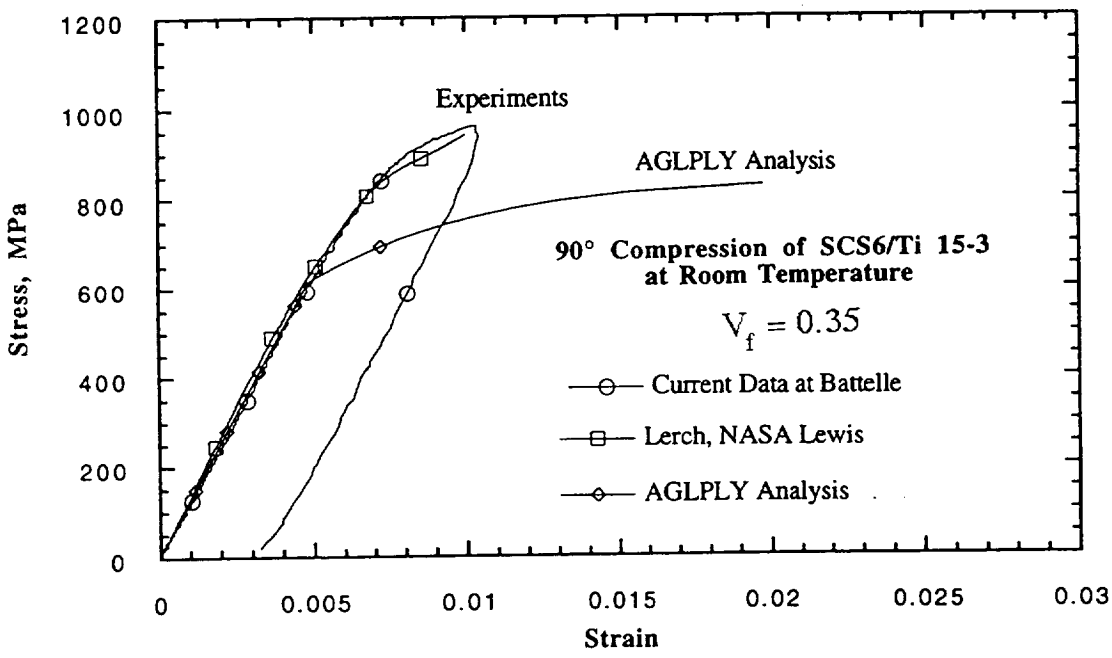

FIGURE 16. AGLPLY ANALYSIS RESULTS FOR $[90]_8$ STRESS-STRAIN RESPONSE IN COMPRESSION

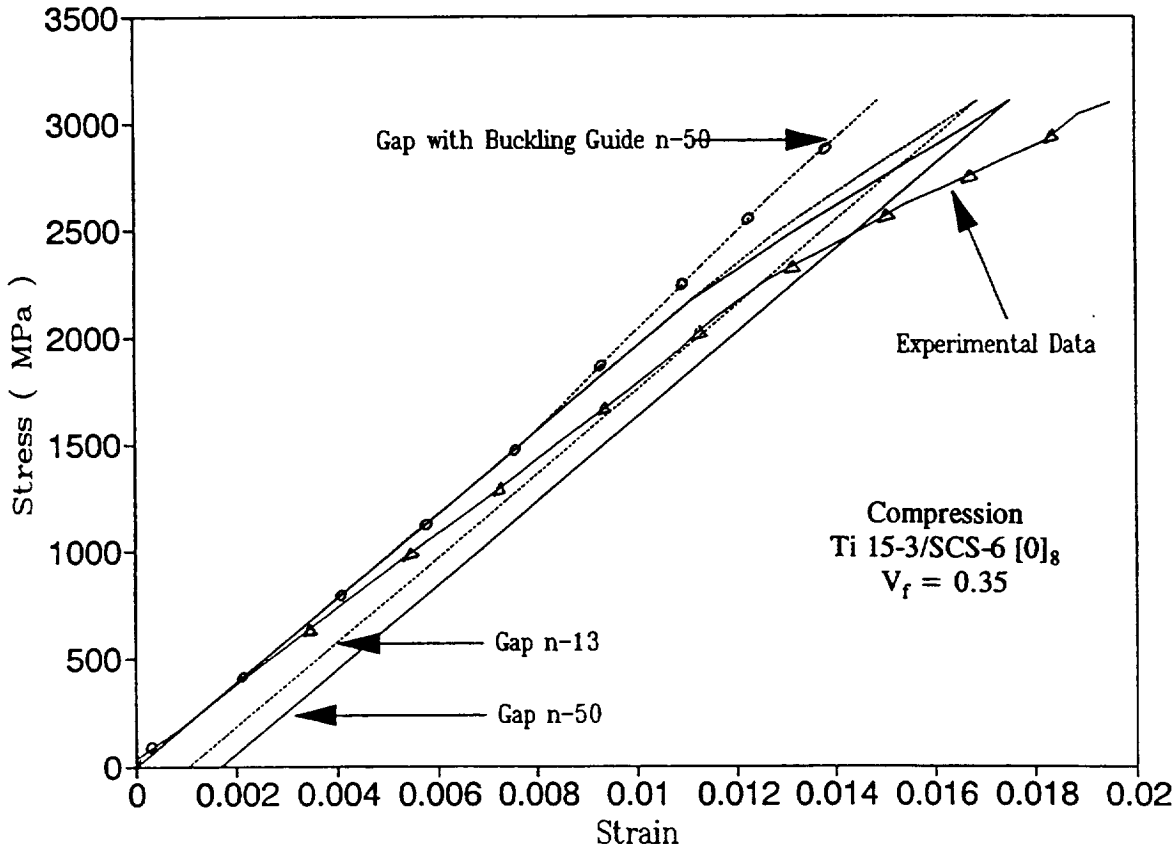

FIGURE 17. BATTELLE'S UNIT CELL COMPUTATIONAL MICROMECHANICS RESULTS FOR $[0]_8$ LAMINA AT RT. VALUES OF n REPRESENT RAMBERG-OSGOOD EXPONENT FOR MATRIX EXPERIMENTAL DATA

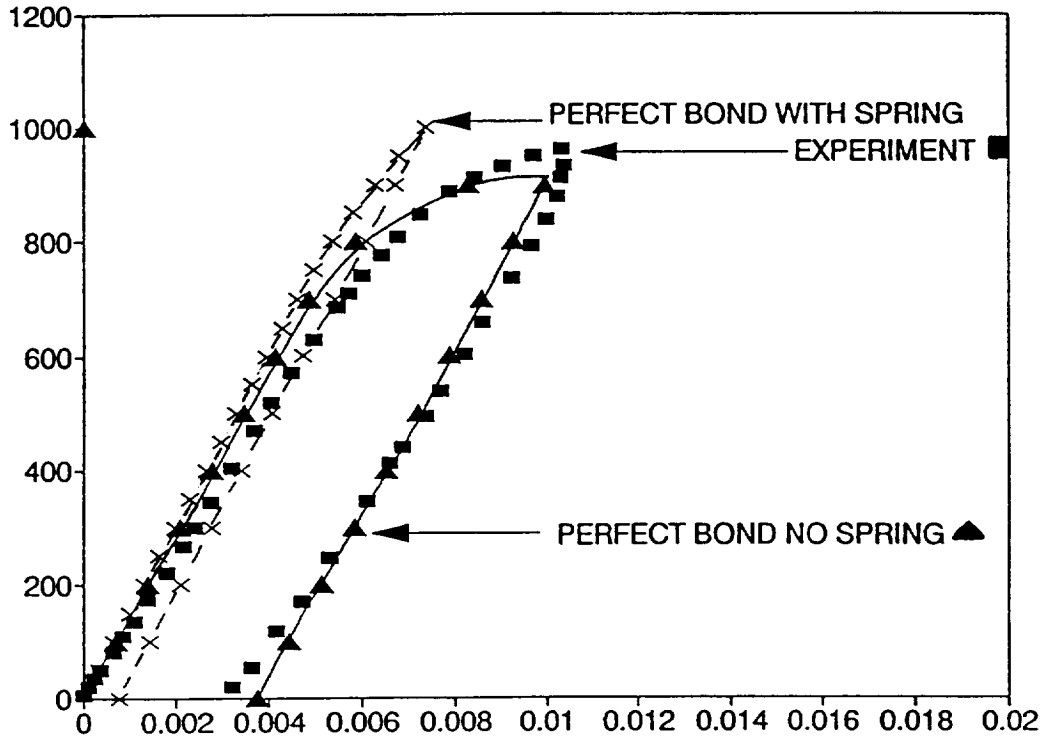

FIGURE 18. BATTELLE'S UNIT CELL COMPUTATIONAL MICROMECHANICS RESULTS FOR $[90]_8$ LAMINA AT RT. LATERAL CONSTRAINT WAS MODELED USING SPRINGS.

REPORT DOCUMENTATION PAGE

Form Approved
OMB No. 0704-0188

1. AGENCY USE ONLY (*Leave blank*)	2. REPORT DATE	3. REPORT TYPE AND DATES COVERED
	September 1993	Final Contractor Report

4. TITLE AND SUBTITLE

Inelastic Deformation Mechanisms in SCS-6/Ti 15–3
MMC Lamina Under Compression

5. FUNDING NUMBERS

WU–510–01–50
C–NAS3–26494

6. AUTHOR(S)

Golam M. Newaz and Bhaskar S. Majumdar

7. PERFORMING ORGANIZATION NAME(S) AND ADDRESS(ES)

Battelle Memorial Institute
505 King Ave.
Columbus, Ohio 43201–2693

8. PERFORMING ORGANIZATION REPORT NUMBER

E–8085

9. SPONSORING/MONITORING AGENCY NAME(S) AND ADDRESS(ES)

National Aeronautics and Space Administration
Lewis Research Center
Cleveland, Ohio 44135–3191

10. SPONSORING/MONITORING AGENCY REPORT NUMBER

NASA CR–191170

11. SUPPLEMENTARY NOTES

Project Manager, Brad Lerch, Structures Division, (216) 433–5522.

12a. DISTRIBUTION/AVAILABILITY STATEMENT

Unclassified - Unlimited
Subject Category 24

12b. DISTRIBUTION CODE

13. ABSTRACT (*Maximum 200 words*)

An investigation was undertaken to study the inelastic deformation mechanisms in $[0]_8$ and $[90]_8$ Ti 15-3/SCS-6 lamina subjected to pure compression. Monotonic tests were conducted at room temperature (RT), 538 °C and 650 °C. Results indicate that mechanical response and deformation characteristics were different in monotonic tension and compression loading whereas some of those differences could be attributed to residual stress effects. There were other differences because of changes in damage and failure modes. The inelastic deformation in the $[0]_8$ lamina under compression was controlled primarily by matrix plasticity, although some evidence of fiber-matrix debonding was observed. Failure of the specimen in compression was due to fiber buckling in a macroscopic shear zone (the failure plane). The inelastic deformation mechanisms under compression in $[90]_8$ lamina were controlled by radial fiber fracture, matrix plasticity and fiber-matrix debonding. The radial fiber fracture was a new damage mode observed for MMCs. Constitutive response was predicted for both the $[0]_8$ and $[90]_8$ laminae, using AGLPLY, METCAN and Battelle's Unit Cell FEA model. Results from the analyses were encouraging.

14. SUBJECT TERMS

Metal matrix composite; Compression; SiC/Ti-15–3;Deformation; Damage

15. NUMBER OF PAGES

35

16. PRICE CODE

A03

17. SECURITY CLASSIFICATION OF REPORT	18. SECURITY CLASSIFICATION OF THIS PAGE	19. SECURITY CLASSIFICATION OF ABSTRACT	20. LIMITATION OF ABSTRACT
Unclassified	Unclassified	Unclassified	